Research Square

Preprints are preliminary reports that have not undergone peer review.
They should not be considered conclusive, used to inform clinical practice,
or referenced by the media as validated information.

A Novel Cobalt Chloride-Induced Prostate Hypoxia Model in Rats

Zhang Qinyu
Zhejiang Chinese Medical University
Xuan Yang
Second Affiliated Hospital of Zhejiang Chinese Medical University
Zhang Hao
Second Affiliated Hospital of Zhejiang Chinese Medical University
Duan Yue
dyurology@163.com

Second Affiliated Hospital of Zhejiang Chinese Medical University

Article

Keywords: prostate hypoxia, cobalt chloride, animal model, HIF-1α

Posted Date: August 10th, 2026

DOI: https://doi.org/10.21203/rs.3.rs-10167753/v1

License: This work is licensed under a Creative Commons Attribution 4.0 International License.
Read Full License

Additional Declarations: No competing interests reported.

Abstract

Background: Chronic prostatitis/chronic pelvic pain syndrome (CP/CPPS) is a common and refractory disease in urology, with a complex pathogenesis involving inflammation, neural dysregulation, and microcirculatory disorders. Recent evidence highlights tissue hypoxia as a key pathophysiological mechanism. Hypoxia-inducible factor-1α (HIF-1α) stabilizes under hypoxic conditions and activates downstream genes related to inflammation and fibrosis, forming a “hypoxia-inflammation” vicious cycle. However, existing animal models (e.g., bacterial infection, hormone-induced, autoimmune models) primarily induce inflammation as a cause rather than a consequence of hypoxia, making it difficult to study hypoxia as an initial driver. Physical hypoxic chambers induce systemic hypoxia and are costly. Therefore, a model that directly and specifically induces localized prostatic hypoxia is urgently needed. In this study, we innovatively establish a novel rat model of prostatitis driven by hypoxia using cobalt chloride ($CoCl_2$) chemical induction, with a “local priming + systemic amplification” strategy. This technical report aims to describe and validate this model.

Methods: Male Sprague-Dawley rats (250–350g) were randomly divided into sham and model groups (n=6/group). On Day 0, rats in the model group received multi-point intraprostatic capsule injection of $CoCl_2$ (5 mg/kg, 100 μL per point) under anesthesia, while sham rats received equal volume of saline. On Days 1 and 2, model rats received intraperitoneal injections of $CoCl_2$ (10 mg/kg) for systemic amplification. On Day 3, prostate tissues were collected. Model validation included: (1) Hematoxylin-eosin (HE) staining for histopathological changes; (2) Western blot for HIF-1α protein expression; (3) ELISA for pro-inflammatory cytokines (TNF-α, IL-1β, IL-6). Data were analyzed by unpaired Student’s t-test ($P < 0.05$ considered significant).

Results: Compared with the sham-operated group, the model group exhibited marked histopathological changes in the prostate, including hydropic degeneration, necrosis and shedding of epithelial cells, and extensive inflammatory cell infiltration, with a significantly elevated inflammation score ($^*p^* < 0.05$). Both immunohistochemistry and Western blot analyses revealed a significant upregulation of hypoxia-inducible factor-1α (HIF-1α) protein expression in the model group ($^*p^* < 0.05$). Western blot also showed increased cleaved caspase-1 levels, indicating inflammasome activation. ELISA demonstrated that the concentrations of pro-inflammatory cytokines IL-1β, IL-6, and TNF-α in prostate tissues were significantly higher in the model group than in the sham group ($^*p^* < 0.05$). Collectively, these results confirm that combined intraperitoneal and intraprostatic injection of cobalt chloride successfully establishes a rat model of prostate hypoxia and inflammation.

Conclusion: Local injection of cobalt chloride can construct hypoxic inflammation model of rat prostate, which has the advantages of targeting, minimally invasive and simple, and provides a reliable platform for the study of prostate disease mechanism and drugs.

Introduction

Chronic prostatitis/chronic pelvic pain syndrome (CP/CPPS) is a common and challenging urological condition with a complex pathogenesis involving inflammation, neural dysregulation, and local microcirculatory disorders[1, 2]. In recent years, tissue hypoxia has gained increasing attention as a critical pathophysiological mechanism in prostatitis. Studies indicate that chronic prostatic inflammation is often accompanied by microvascular dysfunction and reduced blood flow, leading to decreased tissue oxygen tension and the formation of a hypoxic microenvironment. Hypoxia-inducible factor-1α (HIF-1α) is the central transcription factor that senses and adapts to hypoxia; its stabilisation activates downstream genes related to inflammation, angiogenesis, and fibrosis, thereby creating a "hypoxia–inflammation" vicious cycle that promotes disease chronicity[3–6]. Therefore, elucidating the role of hypoxia in prostatitis is important for uncovering pathological mechanisms and identifying new therapeutic targets.

Currently used animal models for prostatitis mainly include bacterial infection, hormone-induced, and autoimmune models[1]. Although these models reproduce some inflammatory features of human disease, they are inadequate for recapitulating the specific hypoxic component. For example, the classical oestrogen-plus-castration non-bacterial prostatitis model primarily addresses hormonal imbalance and immune responses, whereas bacterial infection models focus on acute pathogen-driven inflammation. While these models can show secondary elevations in hypoxia markers (e.g., HIF-1α)[1], hypoxia appears as a consequence rather than an initiator of inflammation, making it difficult to precisely study how hypoxia as an initial trigger provokes and amplifies prostatic inflammatory cascades. Moreover, physical hypoxic chambers produce systemic hypoxia, lack prostate-specific local control, are expensive, and are technically demanding. Hence, there is an urgent need for an animal model that directly and specifically induces localised prostatic hypoxia to investigate its interplay with inflammation.

In this study, we innovatively employ cobalt chloride ($CoCl_2$), a well-recognised chemical hypoxia-mimetic agent that stabilises HIF-1α by competing with haem iron in oxygen sensors, thereby simulating hypoxic molecular and cellular effects under normoxic conditions[6–8]. Our model design incorporates a dual innovation: on Day 0, a low dose of $CoCl_2$ (5 mg/kg) is injected into multiple subcapsular sites of the prostate to establish an initial local hypoxic stimulus; on Days 1 and 2, a higher dose (10 mg/kg) is administered intraperitoneally for systemic reinforcement, mimicking a sustained and amplified hypoxic stress. This "local priming + systemic amplification" strategy aims to better approximate the clinical scenario of progressive ischaemic hypoxia in the prostate.

The purpose of this technical report is to describe and validate this novel SD rat model of prostatic hypoxia. By integrating molecular, biochemical, and histopathological data, we aim to systematically reveal the role of hypoxia as a driving factor in prostatitis and to provide a reliable experimental platform for future mechanism-based and intervention-based studies.

Materials and Methods

1. Reagents and antibodies

Cobalt chloride ($CoCl_2$) was purchased from Macklin (cat. no. C804815). A stock solution (10 mg/mL) was prepared in sterile saline, filter-sterilised, and stored at 4°C in the dark. Working solutions for intraperitoneal and subcapsular injections were diluted from this stock.

ELISA kits for tumour necrosis factor-α (TNF-α), interleukin-1β (IL-1β), and interleukin-6 (IL-6) were obtained from Kequn (cat. nos. KQ-E1017Ra, KQ-E1009Ra, and KQ-E1343Ra, respectively). All procedures were performed strictly according to the manufacturers' instructions.

Primary antibodies: rabbit anti-rat HIF-1α polyclonal antibody (Affinity, cat. no. AF1009) was used at 1:1000; mouse anti-β-actin monoclonal antibody (Lablead, cat. no. A0101) was used as the loading control at 1:5000. Horseradish peroxidase (HRP)-conjugated goat anti-rabbit IgG (cat. no. 7074) and goat anti-mouse IgG (cat. no. 7076) were from Cell Signaling Technology, both at 1:1000.

Other reagents: RIPA lysis buffer, BCA protein assay kit, and ECL chemiluminescent substrate were from Thermo Fisher Scientific. 4% paraformaldehyde, haematoxylin, eosin, and other histology reagents were purchased from Servicebio (Wuhan, China).

2. Experimental animals

Healthy, sexually mature male Sprague-Dawley (SD) rats (250–350 g, approximately 8–11 weeks old) were obtained from Shanghai BK Company. All animals were housed in a specific pathogen-free (SPF) facility under controlled conditions (22 ± 2°C, 55 ± 10% humidity, 12-h light/dark cycle) with free access to standard chow and water[9,10]. After at least one week of acclimatisation, the experiments were initiated. All animal procedures were conducted in strict accordance with the Regulations for the Administration of Laboratory Animals (National Science and Technology Commission of China), the Guidelines for the Humane Treatment of Laboratory Animals (Ministry of Science and Technology of China), and the Zhejiang Provincial Regulations on the Management of Laboratory Animals. The study was approved by the Institutional Animal Care and Use Committee of The Second Affiliated Hospital of Zhejiang Chinese Medical University (approval no. IACUC-20260413-29) and followed the ARRIVE guidelines to improve reporting quality [11,12].

3. Intraprostatic subcapsular injection

3.1 Preoperative preparation

Rats were fasted for 12 h with free access to water. Anaesthesia was induced by intraperitoneal injection of 2% pentobarbital sodium (40 mg/kg)[13]. After full anaesthesia, rats were placed supine on a sterile operating table; the lower abdominal area was shaved and disinfected alternately with iodine and 75% ethanol three times.

3.2 Surgical localisation and prostate exposure

A midline lower abdominal incision (approximately 1.5 cm) was made, and the subcutaneous tissue and linea alba were carefully dissected to open the peritoneal cavity. The intestinal loops were gently

retracted cephalad with sterile cotton swabs to expose the genital structures posterior to the bladder neck. The whitish seminal vesicles were identified, and the ventral and dorsolateral prostatic lobes were firmly attached to their bases[5]. The surrounding tissues were protected with sterile moist gauze, and the target prostatic lobes were clearly exposed.

3.3 Subcapsular injection (core procedure)
Injections were performed using a 29-gauge insulin syringe (0.3 mL; BD). The needle bevel was directed upward and inserted at approximately 30° into the subcapsular space of the ventral prostatic lobe to a depth of 1–2 mm. The drug solution (100 μL per site containing $CoCl_2$ 5 mg/kg) was slowly injected. A successful subcapsular injection was indicated by the formation of a localised, pale, bleb-like elevation around the injection site with no obvious extravasation or parenchymal leakage. A total of four sites were injected—both ventral and dorsolateral lobes on each side. Sham-operated rats received equal volumes of sterile saline using the identical procedure. A schematic representation is shown in Figure 1.

3.4 Postoperative care

After injection, the viscera were gently repositioned. The linea alba and muscle layer were closed with continuous 5-0 absorbable sutures, and the skin incision was closed with interrupted sutures. Immediately after surgery, buprenorphine (0.1 mg/kg) was administered subcutaneously for analgesia[12]. Rats were housed individually in warmed cages with clean bedding and monitored until fully awake. Incisions were inspected and disinfected daily for three consecutive days.

4. Experimental grouping

Twelve SD rats were randomly divided into two groups (n = 6 per group) using a random number table:

Sham group: received multipoint subcapsular injections of sterile saline (100 μL per site) and intraperitoneal injections of equal-volume saline on Days 1 and 2.

Model group: received multipoint subcapsular injections of $CoCl_2$ solution (5 mg/kg in 100 μL saline per site) on Day 0, and intraperitoneal injections of $CoCl_2$ (10 mg/kg) on Days 1 and 2 for reinforcement.

5. Specimen collection

At 24 h after the last intraperitoneal injection (i.e., Day 3), rats were euthanised by CO_2 asphyxiation. The entire prostate complex was rapidly excised and placed in pre-chilled saline. Ventral and dorsolateral lobes were carefully separated on ice. The prostate tissue from each rat was divided into two portions: one was snap-frozen in liquid nitrogen and stored at –80°C for Western blotting and ELISA; the other was immediately fixed in 4% paraformaldehyde at 4°C for 24 h for paraffin embedding and HE staining.

6. Model validation methods

6.1 Haematoxylin and eosin (HE) staining

Fixed tissues were dehydrated through graded ethanol, cleared in xylene, and embedded in paraffin. Serial sections (5 μm thick) were cut, deparaffinised, rehydrated, and stained with haematoxylin and eosin, then mounted with neutral resin. Sections were examined under a light microscope (Nikon Eclipse 80i) by two pathologists blinded to the group assignments. Inflammatory cell infiltration, interstitial oedema, and glandular structural disruption were evaluated [14].

The severity of prostatic histopathological changes was quantitatively assessed by the same two independent pathologists using a semi-quantitative scoring system (grades 0–3) that comprehensively evaluated two core parameters: (1) epithelial injury (including hydropic degeneration, necrosis, and shedding) and (2) interstitial inflammatory cell infiltration. The specific definitions were as follows:

Grade 0: Normal prostate architecture; intact monolayer columnar epithelium with uniform cytoplasm; no obvious interstitial oedema or inflammatory cells.

Grade 1 (Mild): Focal epithelial vacuolation or mild hydropic degeneration; slight interstitial widening; scattered lymphocytes or neutrophils in the stroma.

Grade 2 (Moderate): Apparent epithelial disruption with multifocal necrosis and shedding; moderate interstitial oedema; multifocal aggregations of inflammatory cells.

Grade 3 (Severe): Extensive epithelial necrosis with abundant luminal debris; marked destruction of acinar structures; dense, diffuse infiltration of inflammatory cells (lymphocytes and neutrophils) accompanied by early fibrotic changes.

The final score for each specimen was the average of the two observers' scores, and the mean ± SD was calculated for each group.

6.2 Western blotting

Frozen prostate tissues were homogenised in RIPA lysis buffer containing protease inhibitors. After centrifugation, the supernatant was collected, and protein concentration was determined using the BCA method. Equal amounts of protein (30 μg) were separated by 10% SDS-PAGE and transferred onto PVDF membranes. Membranes were blocked with 5% non-fat milk at room temperature for 1 h, then incubated with primary antibodies overnight at 4°C. After washing with TBST, membranes were incubated with HRP-conjugated secondary antibodies for 1 h at room temperature. Signals were visualised with ECL substrate and captured on a ChemiDoc imaging system (Bio-Rad). Densitometric analysis was performed using ImageJ (NIH); relative expression was expressed as the ratio of target protein (HIF-1α) to β-actin [5].All western blot images were acquired using a ChemiDoc imaging system (Bio-Rad) and processed with ImageLab software (Bio-Rad). Brightness and contrast adjustments were applied equally to the entire image. No nonlinear adjustments or manipulations (e.g., cloning, healing, or threshold manipulation) were performed.

6.3 ELISA

The other frozen tissue portion was homogenised in pre-chilled PBS (w/v), centrifuged, and the supernatant was collected. TNF-α, IL-1β, and IL-6 concentrations were measured using the respective ELISA kits according to the manufacturers' protocols. Absorbance was read at 450 nm, and cytokine concentrations were calculated from standard curves, expressed as picograms per milligram of tissue protein (pg/mg protein).

6.4 Statistical analysis

All data are presented as mean ± standard deviation (SD). Statistical analyses were performed using GraphPad Prism 9.0. Comparisons between two groups were made using unpaired Student's t-test. A P-value < 0.05 was considered statistically significant [10].

Results

1. General observations and injection outcome

All rats survived to the endpoint (survival rate 100% in both groups, 6/6 each). In the model group, body weight slightly decreased on postoperative Day 1 (approximately 3.2% reduction from baseline) but gradually recovered from Day 3 onward, with no statistically significant difference compared with the sham group (P > 0.05). Gross inspection showed no obvious redness, exudation, or purulent infection at the injection sites. On dissection, mild periprostatic adhesions were observed, but no focal necrosis was seen at the injection points.

2. Histopathological changes (HE staining)

Prostate HE staining results are shown in Figure 2. At low magnification (×40), sham group showed clear acinar structures with well-aligned epithelial cells and no interstitial inflammatory infiltrates; the model group displayed disrupted acinar architecture and widened interstitium. At high magnification (×200), sham group exhibited a monolayer of columnar epithelium with uniform cytoplasm and basally located nuclei; the model group showed marked pathological alterations: widespread hydropic degeneration (cell swelling, clear cytoplasm), focal epithelial necrosis and shedding, intraluminal necrotic debris, and dense infiltration of lymphocytes and neutrophils in the interstitium, accompanied by mild fibrotic changes. Semi-quantitative scoring confirmed a significant increase in inflammation score in the model group compared with sham (**P < 0.001; Figure 2B).

3. Inflammatory cytokine levels (ELISA)

ELISA results are presented in Figure 3. Prostatic concentrations of IL-1β, IL-6, and TNF-α were all significantly higher in the model group than in the sham group (P < 0.05 for each).

4. Protein expression of HIF-1α and inflammasome components (Western blotting)

Western blotting was performed to assess HIF-1α, ASC (apoptosis-associated speck-like protein containing a CARD), caspase-1, and cleaved caspase-1 (Figure 4). The model group showed a marked increase in HIF-1α band intensity, with relative expression approximately 2.8-fold higher than sham (**P < 0.001). Caspase-1 and cleaved caspase-1 levels were also significantly upregulated, while ASC exhibited a modest decrease (P* < 0.05), possibly reflecting its oligomerisation and consumption during inflammasome activation (see Discussion).

5. Immunohistochemical localisation of HIF-1α

Immunohistochemical staining for HIF-1α is shown in Figure 5. In the sham group, prostate epithelial cells exhibited weak or negative staining in both cytoplasm and nuclei. In the model group, most epithelial cells showed intense brown positive staining in nuclei and cytoplasm, with dense distribution. Quantitative optical density analysis confirmed a significant increase in the model group (P < 0.05).

Discussion

In this study, we established a novel rat model of prostatic hypoxia and inflammation induced by a combination of intraperitoneal and subcapsular $CoCl_2$ administration. The model's validity is supported by multiple lines of evidence: Western blotting and immunohistochemistry showed significantly elevated HIF-1α protein expression in the prostate (**P < 0.001), confirming that $CoCl_2$ successfully mimicked a local hypoxic microenvironment [15, 16]. Concurrently, Western blotting revealed increased cleaved caspase-1 and a modest reduction in ASC (likely due to ASC speck formation and consumption), suggesting activation of the NLRP3 inflammasome—a key mechanism linking hypoxia to sterile inflammation. ELISA confirmed significantly higher IL-1β, IL-6, and TNF-α concentrations in the model group (P* < 0.05) [17–19]. HE staining demonstrated extensive epithelial hydropic degeneration, necrosis, shedding, and dense inflammatory infiltration, with a markedly elevated inflammation score (***P < 0.001). Collectively, these findings indicate that the model successfully recapitulates a local hypoxia-driven inflammatory cascade [20–22].

Currently, commonly used prostate hypoxia/inflammation models include surgical ligation (e.g., urethral or vas deferens ligation causing urine reflux) and systemic administration (e.g., intraperitoneal $CoCl_2$ or lipopolysaccharide) [23]. To objectively position our model's advantages and limitations, we compared it with these classical approaches across multiple dimensions. Surgical ligation requires sophisticated microsurgical skills and has a long modelling period (2–4 weeks for chronic inflammation), with high animal trauma and risk of urinary obstruction or hydronephrosis. Systemic administration is technically easy and rapid but causes non-specific systemic hypoxia. Our model involves moderate-difficulty subcapsular injection, yields acute responses within days, and causes only minimal puncture trauma and abdominal incision; postoperative activity, feeding, and urination were normal, with significantly less suffering than ligation models, aligning with the "reduction" principle of the 3Rs[27]. Moreover, our "local + systemic" strategy achieves prostate targeting while providing a systemic hypoxic background, reducing off-target effects on vital organs. Reproducibility is high, and costs are moderate.

However, the model has limitations[24–26]. First, it is an acute injury model with a 3-day observation window, reflecting acute hypoxia–inflammation rather than the chronic fibrotic remodelling seen in clinical prostatitis or benign prostatic hyperplasia. Second, $CoCl_2$ may have off-target effects; although subcapsular injection retains most drug locally, some absorption via capsular vessels occurs, and intraperitoneal $CoCl_2$ could impose hepatic or renal toxicity, which requires future quantification via blood cobalt and organ function tests. Third, we did not assess prostate function (e.g., seminal fluid secretion, voiding pressure, pain behaviour), limiting the model's correlation with clinical phenotypes.

Future improvements could include repeated subcapsular injections (e.g., weekly for 4 weeks) or sustained-release formulations (e.g., $CoCl_2$-loaded microspheres or gelatin sponges) to induce persistent hypoxia and fibrosis, better mimicking chronic prostatitis or hyperplasia. Combining with hormonal or autoimmune components could create multi-factorial models. Conversely, the acute phase of this model offers a window for screening anti-hypoxic or anti-inflammatory drugs and identifying optimal intervention timing.

In summary, our combined intraperitoneal and subcapsular $CoCl_2$ administration effectively induces local prostatic hypoxia and acute inflammation in rats. Compared with existing methods, this model offers targeted delivery, minimal invasiveness, low cost, high reproducibility, and compliance with the 3R principles. Although currently acute, it can be adapted for chronic studies through modified protocols, providing a valuable tool for investigating hypoxia-driven prostatic diseases and evaluating therapeutic candidates.

Conclusion

We have successfully established a novel rat model of prostatic hypoxia and inflammation by combined intraperitoneal and subcapsular $CoCl_2$ injection. The model exhibits typical hypoxic injury and sterile inflammatory responses at histopathological, protein, and cytokine levels. Compared with surgical ligation or systemic administration, it offers superior targeting, ease of operation, short modelling time, low animal distress, and high reproducibility, in line with the 3R principles. This model provides a stable and reliable platform for exploring the role of hypoxia in prostate diseases (e.g., chronic prostatitis, benign prostatic hyperplasia) and for screening anti-hypoxic and anti-inflammatory drug candidates.

Declarations

Funding

This work was supported by Zhejiang Provincial Administration of Traditional Chinese Medicine (Grant No. 1004167).

Author Contribution

Conceptualization, D.Y. and Z.Q.; methodology, Z.Q. and Z.H.; validation, Z.Q. and X.Y.; formal analysis, X.Y. and Z.H.; investigation, Z.Q. and Z.H.; data curation, Z.Q. and X.Y.; writing—original draft preparation, Z.Q.; writing—review and editing, D.Y. and X.Y.; visualization, X.Y.; supervision, D.Y.; project administration, D.Y.; funding acquisition, D.Y. All authors have read and agreed to the published version of the manuscript.

Data Availability

All data generated or analyzed during this study are included in this published article and its supplementary information files. The full-length original western blot images are provided in Supplementary Fig. S1. Raw data are available from the corresponding author upon reasonable request.

References

1. He, H., Luo, H., Xu, H., Qian, B., Zou, X., Zhang, G., Zeng, F., & Zou, J. (2023). Preclinical models and evaluation criteria of prostatitis. Frontiers in immunology, 14, 1183895. https://doi.org/10.3389/fimmu.2023.1183895.
2. Shao, B., Wu, K., Fan, Z., Gao, X., Wan, S., Xiao, L., Zuo, Y., Pi, J., & Sun, P. (2026). Current research hotspots and difficulties of chronic prostatitis/chronic pelvic pain syndrome: neuroendocrine mechanism. Annals of medicine, 58(1), 2616886. https://doi.org/10.1080/07853890.2026.2616886.
3. Wang, Y., Lao, Y., Li, R., You, C., Qing, L., Xiao, X., Liu, S., Wang, W., Zhao, Y., & Dong, Z. (2024). Network pharmacological analysis and experimental study of melatonin in chronic prostatitis/chronic pelvic pain syndrome. Naunyn-Schmiedeberg's archives of pharmacology, 397(11), 8691–8706. https://doi.org/10.1007/s00210-024-03183–8.
4. Szymanska, B., Debowski, J., Malkiewicz, B., & Piwowar, A. (2024). Assessment of interleukin 17A and 23 in the course of bladder cancer and selected benign urological diseases. Journal of physiology and pharmacology: an official journal of the Polish Physiological Society, 75(1), 10.26402/jpp.2024.1.08. https://doi.org/10.26402/jpp.2024.1.08.
5. Meng, T., Zhang, Y., Wang, H., Wu, W., Peng, W., Yue, J., Huang, C., Liu, W., Liang, C., Yang, C., & Chen, J. (2025). Irf7 aggravates prostatitis by promoting Hif–1α-mediated glycolysis to facilitate M1 polarization. Cellular and molecular life sciences: CMLS, 82(1), 90. https://doi.org/10.1007/s00018-025-05608-w.
6. Basheeruddin, M., & Qausain, S. (2024). Hypoxia-Inducible Factor 1-Alpha (HIF–1α) and Cancer: Mechanisms of Tumor Hypoxia and Therapeutic Targeting. Cureus, 16(10), e70700. https://doi.org/10.7759/cureus.70700.
7. Bhat, K. M. R., Upadhya, R., Adiga, S., Kumar, S. E. P., Manjula, S. D., Acharya, N., Subramanian, H. H., & Upadhya, D. (2025). Regulation of chronic neuroinflammation through dietary herbal products. Frontiers in nutrition, 12, 1487786. https://doi.org/10.3389/fnut.2025.1487786.

8. Wu, Z. X., Chen, S. S., Lu, D. Y., Xue, W. N., Sun, J., Zheng, L., Wang, Y. L., Li, C., Li, Y. J., & Liu, T. (2023). Shenxiong glucose injection inhibits oxidative stress and apoptosis to ameliorate isoproterenol-induced myocardial ischemia in rats and improve the function of HUVECs exposed to CoCl2. Frontiers in pharmacology, 13, 931811. https://doi.org/10.3389/fphar.2022.931811.
9. National Toxicology Program (2021). Toxicology and carcinogenesis studies of sodium tungstate dihydrate in Sprague Dawley (Hsd:Sprague Dawley SD) rats and B6C3F1/N mice (drinking water studies). National Toxicology Program technical report series, (599), NTP-TR–599. https://doi.org/10.22427/NTP-TR–599.
10. Liu, S., Zhang, B., Ma, S., Wu, F., Shi, X., Wu, J., Jensen, O. T., Cariati, P., Hong, J., & Zhu, X. (2024). The mechanism of bone metabolism in a Sprague Dawley rat model of mandibular osteoradionecrosis. Quantitative imaging in medicine and surgery, 14(7), 4403–4416. https://doi.org/10.21037/qims–24–47.
11. Percie du Sert, N., Hurst, V., Ahluwalia, A., Alam, S., Avey, M. T., Baker, M., Browne, W. J., Clark, A., Cuthill, I. C., Dirnagl, U., Emerson, M., Garner, P., Holgate, S. T., Howells, D. W., Karp, N. A., Lazic, S. E., Lidster, K., MacCallum, C. J., Macleod, M., Pearl, E. J., … Würbel, H. (2020). The ARRIVE guidelines 2.0: Updated guidelines for reporting animal research. PLoS biology, 18(7), e3000410. https://doi.org/10.1371/journal.pbio.3000410.
12. Kilkenny, C., Browne, W., Cuthill, I. C., Emerson, M., Altman, D. G., & NC3Rs Reporting Guidelines Working Group (2010). Animal research: reporting in vivo experiments: the ARRIVE guidelines. British journal of pharmacology, 160(7), 1577–1579. https://doi.org/10.1111/j.1476–5381.2010.00872.x.
13. Routtenberg A. (1968). Pentobarbital anesthesia of albino rats. Journal of the experimental analysis of behavior, 11(1), 52. https://doi.org/10.1901/jeab.1968.11–52.
14. Chen, L., Liu, Y., Yue, S., Wang, H., Chen, J., Ma, W., Xu, W., Xu, M., Chen, Z., Chen, X., Zhang, L., & Liang, C. (2024). P2X7R Modulates NEK7-NLRP3 Interaction to Exacerbate Experimental Autoimmune Prostatitis via GSDMD-mediated Prostate Epithelial Cell Pyroptosis. International journal of biological sciences, 20(9), 3393–3411. https://doi.org/10.7150/ijbs.94704.
15. Saber, S., Abdelhady, R., Elhemely, M. A., Elmorsy, E. A., Hamad, R. S., Abdel-Reheim, M. A., El-Kott, A. F., AlShehri, M. A., Morsy, K., Negm, S., & Kira, A. Y. (2024). Nanoscale Systems for Local Activation of Hypoxia-Inducible Factor–1 Alpha: A New Approach in Diabetic Wound Management. International journal of nanomedicine, 19, 13735–13762. https://doi.org/10.2147/IJN.S497041.
16. Canhasi, L., Tina, E., & Eremo, A. G. (2023). Hypoxia-mimetic by CoCl2 increases SLC7A5 expression in breast cancer cells in vitro. BMC research notes, 16(1), 366. https://doi.org/10.1186/s13104-023-06650–2.
17. Chen, Y., Ye, X., Escames, G., Lei, W., Zhang, X., Li, M., Jing, T., Yao, Y., Qiu, Z., Wang, Z., Acuña-Castroviejo, D., & Yang, Y. (2023). The NLRP3 inflammasome: contributions to inflammation-related diseases. Cellular & molecular biology letters, 28(1), 51. https://doi.org/10.1186/s11658-023-00462–9.

18. Xu, Y., Yang, Y., Chen, X., Jiang, D., Zhang, F., Guo, Y., Hu, B., Xu, G., Peng, S., Wu, L., & Hu, J. (2023). NLRP3 inflammasome in cognitive impairment and pharmacological properties of its inhibitors. Translational neurodegeneration, 12(1), 49. https://doi.org/10.1186/s40035-023-00381-x.
19. Huang, G., Zhang, Y., Zhang, Y., & Ma, Y. (2022). Chronic kidney disease and NLRP3 inflammasome: Pathogenesis, development and targeted therapeutic strategies. Biochemistry and biophysics reports, 33, 101417. https://doi.org/10.1016/j.bbrep.2022.101417.
20. Wu, Z. S., Wang, H. J., Lee, W. C., Luo, H. L., Lin, T. K., & Chuang, Y. C. (2023). Low-Energy Shock Wave Suppresses Prostatic Pain and Inflammation by Modulating Mitochondrial Dynamics Regulators on a Carrageenan-Induced Prostatitis Model in Rats. International journal of molecular sciences, 24(4), 3898. https://doi.org/10.3390/ijms24043898.
21. Zhou, J., Ding, L., Chen, J., Chen, C., Jiang, P., Mei, Z., Jiang, Q., & Hua, X. (2025). HMGB1 Inhibition Alleviates Chronic Nonbacterial Prostatitis by Suppressing M1 Polarization of Macrophages. Journal of inflammation research, 18, 6735–6748. https://doi.org/10.2147/JIR.S502616.
22. Liu, H., Wang, Z., Xie, Q., Chi, A., Li, Y., Dai, J., Zhang, M., Deng, C., & Liu, G. (2022). Ningmitai capsules have anti-inflammatory and pain-relieving effects in the chronic prostatitis/chronic pelvic pain syndrome mouse model through systemic immunity. Frontiers in pharmacology, 13, 949316. https://doi.org/10.3389/fphar.2022.949316.
23. He, H., Luo, H., Xu, H., Qian, B., Zou, X., Zhang, G., Zeng, F., & Zou, J. (2023). Preclinical models and evaluation criteria of prostatitis. Frontiers in immunology, 14, 1183895. https://doi.org/10.3389/fimmu.2023.1183895.
24. Gu, Q., Luan, J., Yu, M., Xia, J., & Wang, Z. (2025). Chronic prostatitis/chronic pelvic pain syndrome impairs erectile function by inducing apoptosis in a rat model of experimental autoimmune prostatitis. International journal of impotence research, 37(7), 519–526. https://doi.org/10.1038/s41443-024-00965–9.
25. Guan, Y., Yue, S., Chen, Y., Cheng, A., Li, H., Yang, F., Liu, Y., Liang, C., & Meng, J. (2025). IGF1R Promotes Th17/Treg Cell Development in Experimental Autoimmune Prostatitis. Journal of inflammation research, 18, 5759–5775. https://doi.org/10.2147/JIR.S508576.
26. Wu, Z. S., Wang, H. J., Lee, W. C., Luo, H. L., Lin, T. K., & Chuang, Y. C. (2023). Low-Energy Shock Wave Suppresses Prostatic Pain and Inflammation by Modulating Mitochondrial Dynamics Regulators on a Carrageenan-Induced Prostatitis Model in Rats. International journal of molecular sciences, 24(4), 3898. https://doi.org/10.3390/ijms24043898.
27. Katsirntaki, K., Hagner, S., Werlein, C., Braubach, P., Jonigk, D., Adam, D., Hidaji, H., Kühn, C., Falk, C. S., Ruhparwar, A., & Wiegmann, B. (2024). Low-Volume Ex Situ Lung Perfusion System for Single Lung Application in a Small Animal Model Enables Optimal Compliance With Reduction in 3R Principles of Animal Research. Transplant international: official journal of the European Society for Organ Transplantation, 37, 13189. https://doi.org/10.3389/ti.2024.13189.

Figures

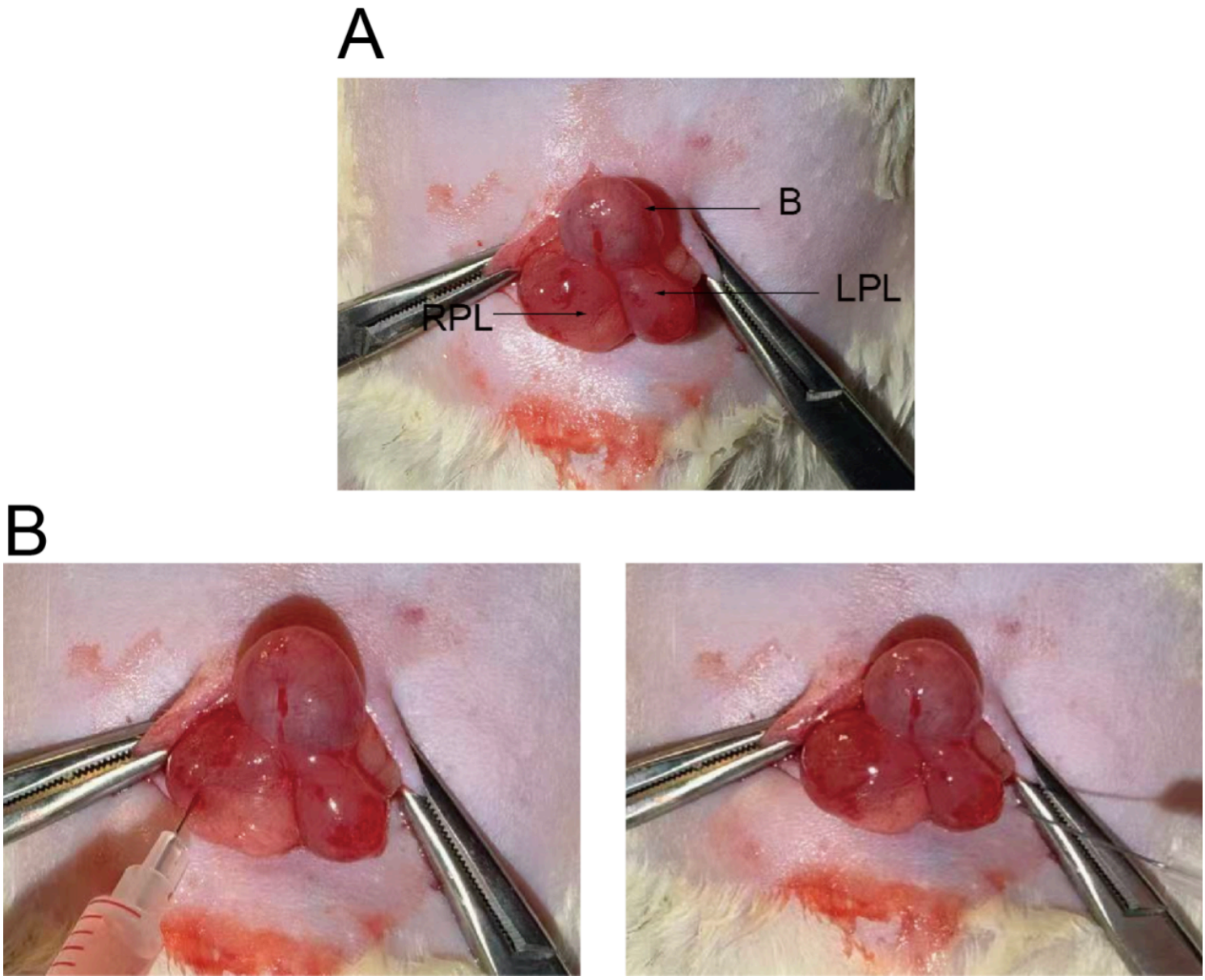


Figure 1

Schematic diagram of subcapsular injection into the rat prostate.
(A) After a midline abdominal incision, the bladder (B), left prostatic lobe (LPL), and right prostatic lobe (RPL) were exposed. (B) Subcapsular injections into the LPL and RPL were performed using a 29-G insulin needle.

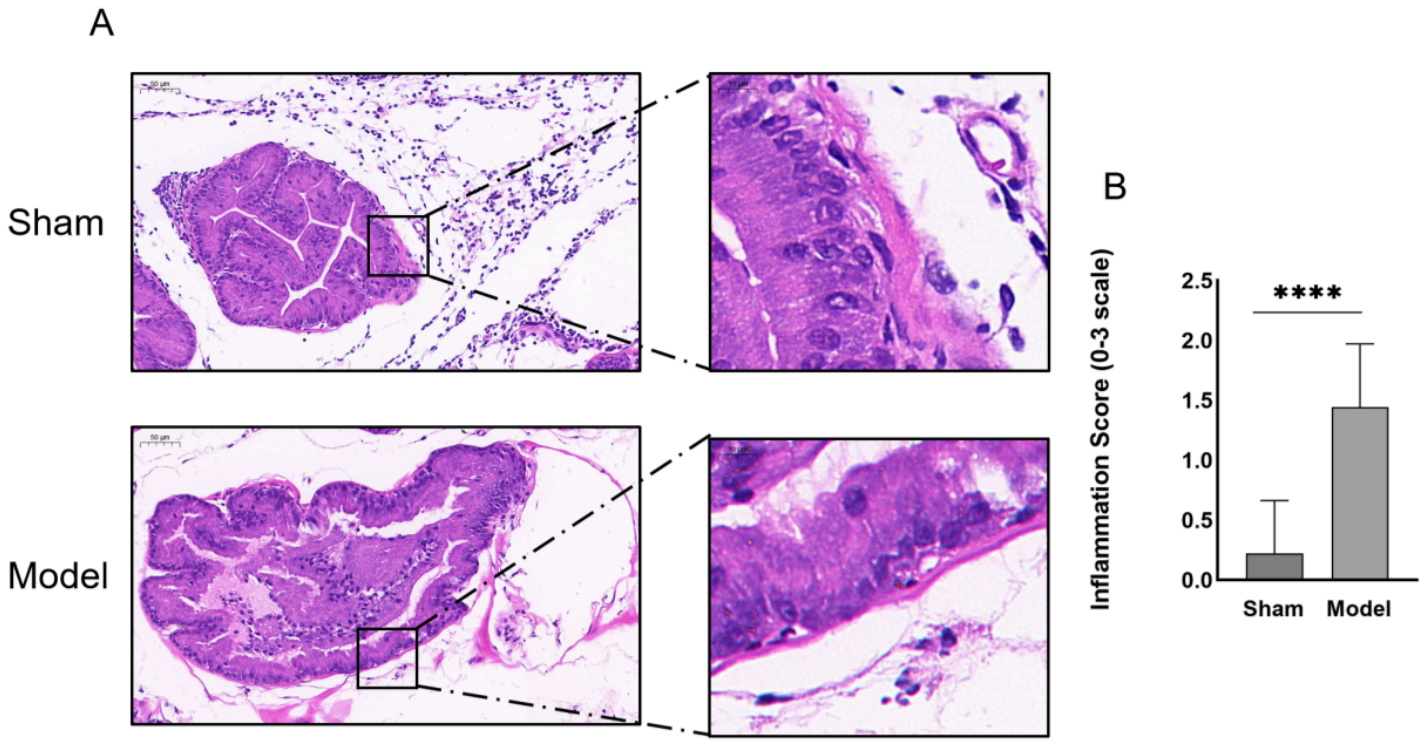


Figure 2

HE staining of prostate tissues.
Prostate sections from sham and model rats were fixed, embedded, sectioned (5 μm), and stained with haematoxylin and eosin. (A) Representative images: low magnification (×40) showing intact acini in sham and disrupted acini with widened interstitium in model; high magnification (×200) showing normal epithelium in sham and hydropic degeneration, necrosis, shedding, and inflammatory infiltration in model. Scale bars: 200 μm (low) and 50 μm (high). (B) Semi-quantitative inflammation scores (0–3, based on epithelial injury and inflammatory infiltration as defined in Methods). Data are mean ± SD (n = 6 per group). **P < 0.001 vs. sham.

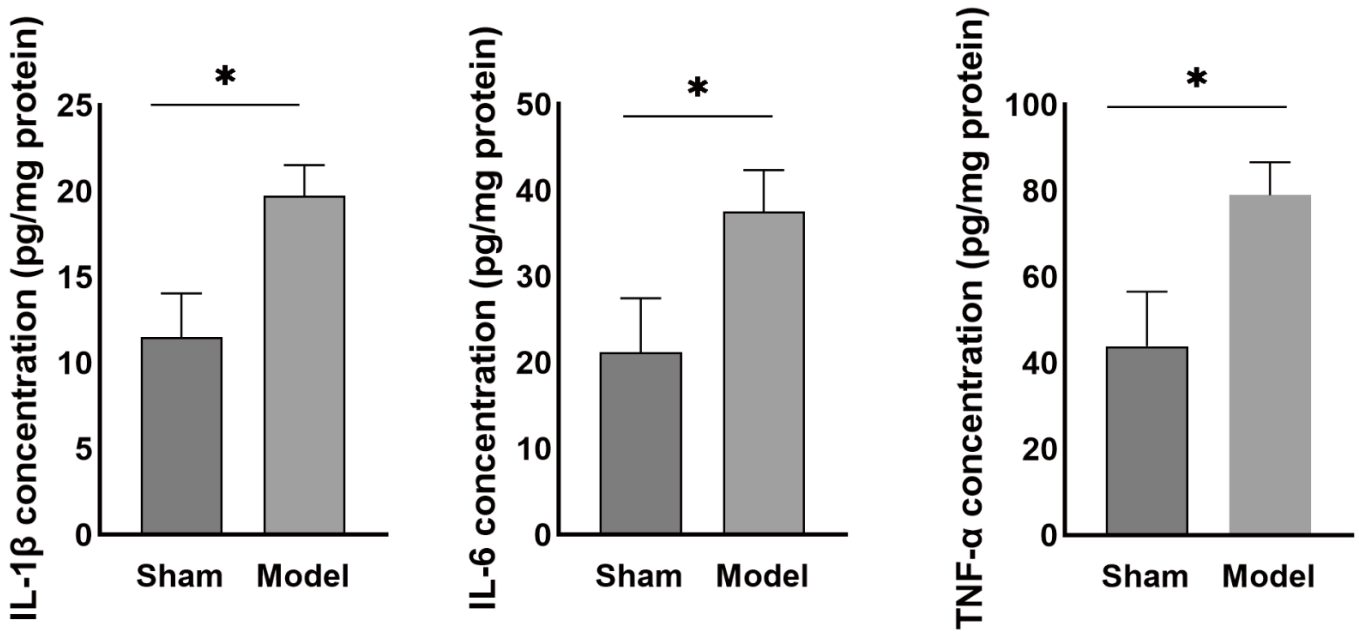


Figure 3

Pro-inflammatory cytokine levels in prostate homogenates (ELISA).
Concentrations of IL-1β, IL-6, and TNF-α were measured by ELISA and expressed as pg/mg protein. Data are mean ± SD (n = 6 per group). $P < 0.05$ vs. sham for all cytokines.

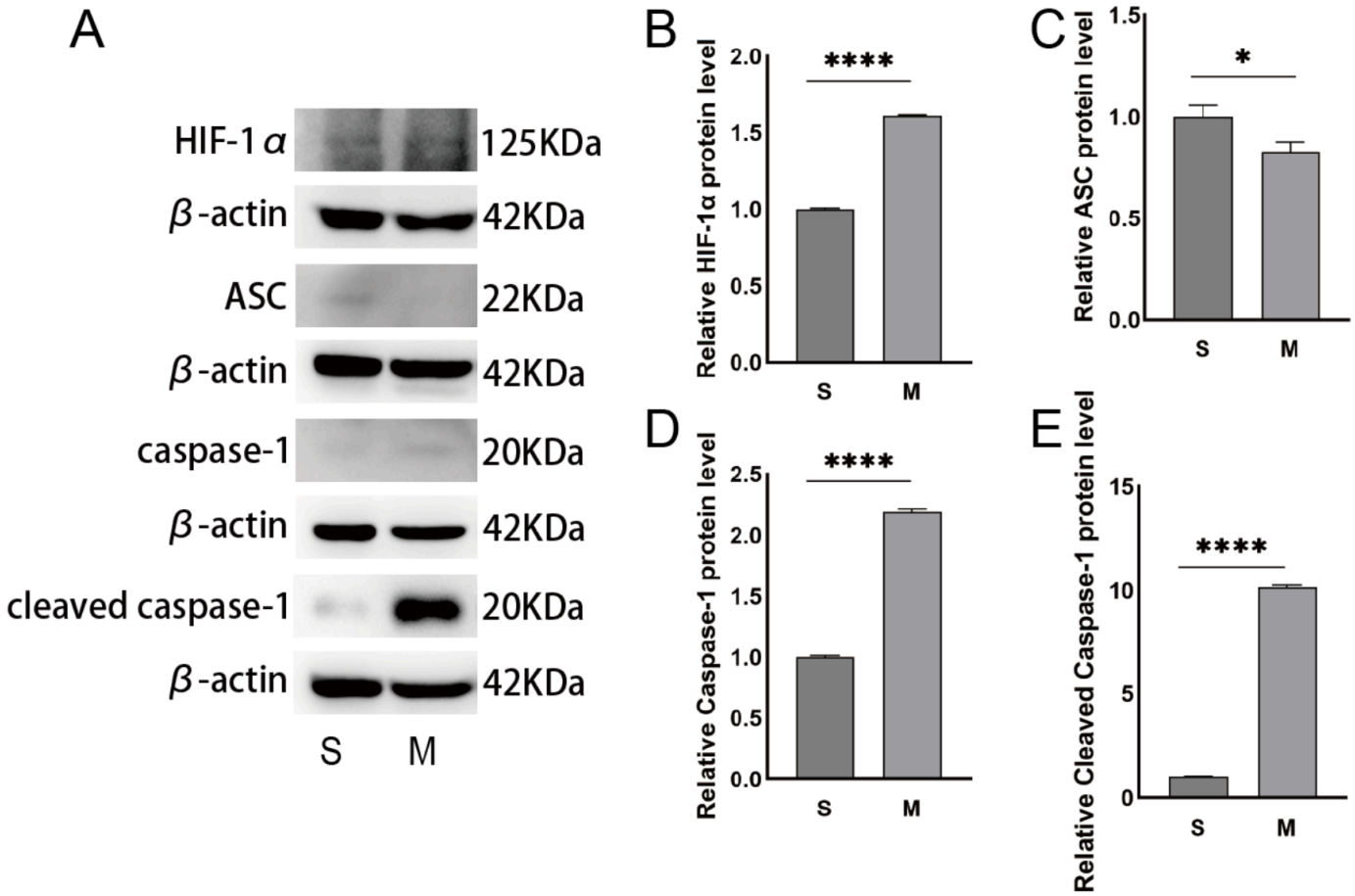


Figure 4

Western blot analysis of HIF-1α, ASC, caspase-1, and cleaved caspase-1.
(A) Representative blots; β-actin served as loading control. S, sham; M, model. Blots were cropped from different parts of the same gel; the cropping boundaries are indicated by white space between lanes. Full-length original blots are provided in Supplementary Fig. S1.(B–E) Densitometric quantification (mean ± SD, n = 6 per group). HIF-1α, caspase-1, and cleaved caspase-1 were significantly elevated (**P < 0.001), while ASC showed a mild reduction (P* < 0.05) in the model group vs. sham.For the purpose of display, the membrane was cut to create the area shown. The complete membrane can be found in the supplementary materials.

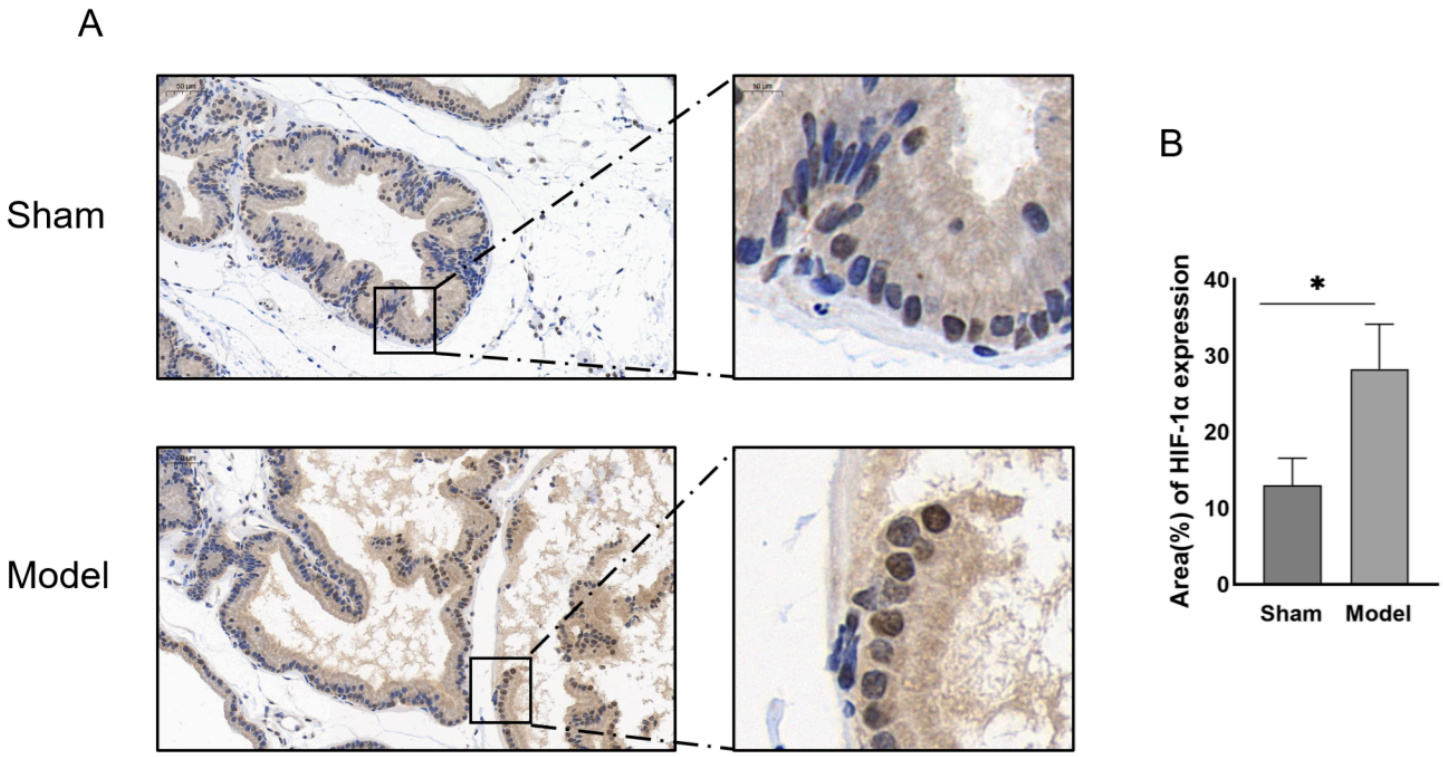


Figure 5

Immunohistochemical staining and optical density analysis of HIF-1α.
(A) Representative images (×200; scale bar = 50 μm): brown granules indicate positive signals. Sham group showed weak or negative staining; model group showed strong brown staining in epithelial nuclei and cytoplasm. (B) Quantitative analysis of mean optical density (IOD/area). Data are mean ± SD (n = 6 per group). $P < 0.05$ vs. sham.

Supplementary Files

This is a list of supplementary files associated with this preprint. Click to download.

- SupplementaryInformationFigureS1.pdf